FISEVIER

Contents lists available at ScienceDirect

Electrochemistry Communications

journal homepage: www.elsevier.com/locate/elecom



The effect of Nafion film on the cathode catalyst layer performance in a low–Pt PEM fuel cell



Andrei Kulikovsky¹

Forschungszentrum Juelich GmbH, Institute of Energy and Climate Research, IEK-3: Electrochemical Process Engineering, Jülich D-52425, Germany

ARTICLE INFO

Keywords:
PEM fuel cell
Low-Pt cathode
Polarization curve
Modeling

ABSTRACT

A single–pore model for performance of the cathode catalyst layer (CCL) in a PEM fuel cell is developed. The model takes into account oxygen transport through the CCL depth and through the thin Nafion film, separating the pore from Pt/C species. Analytical solution to model equations reveals the limiting current density $j_N^{\rm lim}$ due to oxygen transport through the Nafion film. Further, $j_N^{\rm lim}$ linearly depends on the CCL thickness, i.e., the thinner the CCL, the lower $j_N^{\rm lim}$. This result may explain unexpected lowering of low–Pt loaded catalyst layers performance, which has been widely discussed in literature.

1. Introduction

High cost of platinum could potentially slow down development and marketing of low-temperature fuel cells. At present, standard oxygen reduction reaction (ORR) electrode contains 0.4 mg of Pt per square centimeter. This translates to nearly 100 g of precious metal in a 100–kW stack for automotive applications. High Pt cost stimulates worldwide interest in three to fourfold reduction of Pt loading.

As the cell current density j_0 is proportional to Pt surface, one would anticipate a linear decay of j_0 with the Pt loading. However, low-Pt cathodes exhibit unexpected over-linear performance loss (OPL) [1,2]. So far, the reason for this effect is not fully understood. Grezler et al. [1] attributed poor low-Pt cathode performance to oxygen transport through the Nafion film covering Pt/C agglomerates. However, to explain the observed transport resistance, their study has led to unrealistically high Nafion film thickness. Owejan et al. [3] developed a series of cathodes varying Pt loading and keeping the cathode thickness constant. This has been achieved by diluting Pt/C by "pure" carbon particles. Their results, however, did not allow to make a definite conclusion about the OPL nature. Weber and Kusoglu [4] discussed the nature of OPL and provided arguments in favor of the oxygen transport through the Nafion film. Choo et al. [5] have found that the OPL in the low–Pt cathode can partly be mitigated by proper water management of the cell. This work is another indirect evidence that the origin of the OPL is related to oxygen transport in Nafion. Kudo et al. [6] showed that the dominant part of the oxygen transport resistivity in the thin Nafion film is due to Pt/ionomer interface.

Yet, however, the question remains: why oxygen transport in the Nafion film does not affect the performance of standard electrodes with high Pt loading, and it has a strong effect on the performance of low–Pt electrodes? Recent modeling works [7-9] do not give indisputable answer to this question. Chen et al. [10] developed a detailed numerical model of oxygen transport within a single spherical agglomerate, taking into account primary pores and the distribution of Pt species within the agglomerate. They showed that the agglomerate transport resistivity increases with the decrease of Pt loading due to increase in the length of the oxygen mean transport path inside the agglomerate. However, this effect is significant if the rate of oxygen dissolution in Nafion is low, while the respective rate constant is poorly known. In addition, their model employs rather strong assumptions on agglomerate internal structure.

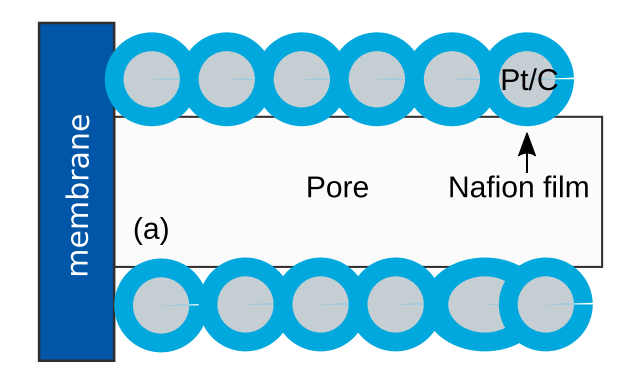
In this work, we report a single–pore model for the cathode catalyst layer (CCL) performance. The model includes oxygen transport in the void pore and in the Nafion film separating the pore from the Pt/C particles. Analytical solution to model equations shows that the polarization curve of this system exhibits limiting current density due to oxygen transport in the Nafion film. Moreover, this limiting current appears to be proportional to the CCL thickness. This effect may explain OPL of low–Pt electrodes, as these electrodes are typically three– to four times thinner, than the standard Pt/C systems.

2. Performance equations

Schematic of a single mesopore in the cathode catalyst layer (CCL) is shown in Fig. 1a. SEM pictures show that in a real CCL, the pore walls

E-mail address: A.Kulikovsky@fz-juelich.de.

¹ ISE member.



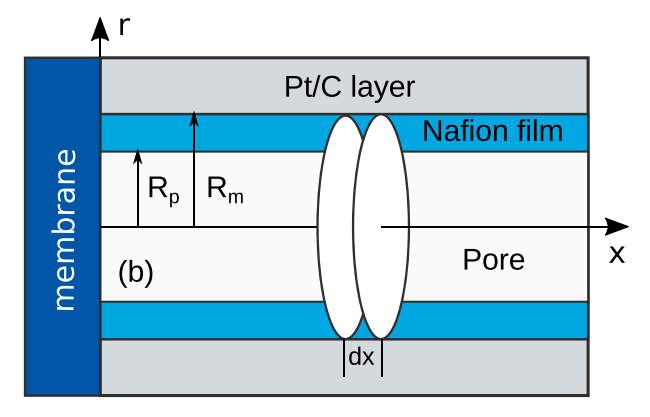


Fig. 1. (a) Schematic of a single pore in the CCL, (b) the system for modeling.

are formed by numerous agglomerates of Pt/C particles, surrounded by a thin Nafion film [11]. It is assumed that the Pt/C clusters have electric contact between them for transport of electrons to the ORR sites.

To model this system, we consider a cylindrical pore depicted in Fig. 1b. The system is formed by three coaxial tubes: void, Nafion film and Pt/C, as shown in Fig. 1b. Let the void pore radius be R_p and the Pt/C radius be R_m (Fig. 1). It is assumed that the system shown in Fig. 1 is a representative pore penetrating through the whole CCL thickness. The pore considered is straight; however, the through–plane oxygen diffusion coefficient can be corrected for real pore tortuosity by a simple correction factor. Note also that the electrochemically active surface area is represented by the side surface of the metal cylinder (Fig. 1). This surface is proportional to the pore length, i.e., to the catalyst layer thickness, as in real Pt/C electrodes.

To write down equations for the pore performance, we need an oxygen flux balance equation in the pore. Consider a cylindrical element of the pore volume of the radius R_m and the thickness dx (Fig. 1b). The oxygen diffusive flux along the pore is $D_p\partial$ c/∂ x, where D_p is the oxygen diffusion coefficient in the pore volume, and c is the local oxygen concentration in the pore. As c(x) decays toward the membrane, the balance of fluxes in the volume element is

$$-\left(\pi R_p^2 D_p \frac{\partial c}{\partial x}\right)_{x+dx} + \left(\pi R_p^2 D_p \frac{\partial c}{\partial x}\right)_x = (2\pi R_m dx) N_{N,m} \tag{1}$$

where

$$N_{N,m} = \left(D_N \frac{\partial c_N}{\partial r}\right)_{r=R_m} \tag{2}$$

is the radial oxygen flux at the metal/Nafion interface consumed in the ORR, c_N is the dissolved oxygen concentration in the Nafion film and D_N is the oxygen diffusion coefficient in the film. Note that D_N is the effective parameter, which includes interfacial Nafion resistance.

Dividing both sides of Eq. (1) by $\pi R_p^2 dx$, we come to

$$-D_{p}\frac{\partial^{2}c}{\partial x^{2}} = \frac{2R_{m}N_{N,m}}{R_{p}^{2}}, \quad \frac{\partial c}{\partial x}\Big|_{x=0} = 0, \quad c(l_{t}) = c_{1},$$
(3)

where c_1 is the oxygen concentration at the CCL/gas diffusion layer (GDL) interface, and l_t is the CCL thickness.

Oxygen transport through the Nafion film along the radial direction is described by

$$-\frac{D_N}{r}\frac{\partial}{\partial r}\left(r\frac{\partial c_N}{\partial r}\right) = 0, \quad c_N(R_p) = K_H c(x),$$

$$D_N\frac{\partial c_N}{\partial r}\Big|_{r=R_m} = -\frac{i_*R_p^2}{2R_m(4F)}\left(\frac{c_{N,m}}{c_{ref}}\right) \exp\left(\frac{\eta}{b}\right)$$
(4)

Here, K_H is the dimensionless Henry constant (mol/mol) for oxygen solubility in Nafion, $c_{N,m} \equiv c_N(R_m)$, i_* is the ORR volumetric exchange current density, and c_{ref} is the reference oxygen concentration. The first boundary condition in Eq. (4) is obvious, while the second means that the oxygen flux at the Nafion/Pt interface equals the flux consumed in the ORR at the Pt surface. This flux is given by the product of the Tafel ORR rate

$$\frac{i_*}{4F} \left(\frac{c_{N,m}}{c_{ref}} \right) \exp \left(\frac{\eta}{b} \right)$$

by the characteristic length $R_p^2/(2R_m)$. This relation provides correct transition to the limiting case of vanishing Nafion film. Indeed, setting $K_H = 1$, $R_p = R_M$, we may omit Eq. (4), set $c_N = c$ and substitute the flux on the right side of the second boundary condition in Eq. (4) instead of $N_{N,m}$ into Eq. (3). This gives

$$-D_{p}\frac{\partial^{2}c}{\partial x^{2}} = -\frac{i_{*}}{4F} \left(\frac{c}{c_{ref}}\right) \exp\left(\frac{\eta}{b}\right), \tag{5}$$

which is a standard macrohomogeneous model (MHM) equation for oxygen transport in the CCL. The system of Eqs. (3), (4) is completed by the proton current conservation equation in the Nafion film:

$$\frac{\partial j}{\partial x} = -i_* \left(\frac{c_{N,m}}{c_{ref}} \right) \exp\left(\frac{\eta}{b} \right) \tag{6}$$

To simplify calculations we introduce dimensionless variables

$$\widetilde{x} = \frac{x}{l_t}, \widetilde{j} = \frac{j}{j_p}, \widetilde{\eta} = \frac{\eta}{b}, \widetilde{r} = \frac{r}{l_t}, \ \widetilde{c} = \frac{c}{c_{ref}}$$
(7)

where

$$j_p = \frac{\sigma_p b}{l_t} \tag{8}$$

is the characteristic current density for proton transport, σ_p is the Nafion film proton conductivity, and b is the ORR Tafel slope. With these variables Eqs. (3), (4) and (6) transform to

$$-\varepsilon_*^2 \widetilde{D}_{0x} \frac{\partial^2 \widetilde{c}}{\partial \widetilde{x}^2} = \varepsilon \varepsilon_*^2 \widetilde{N}_{N,m}, \quad \frac{\partial \widetilde{c}}{\partial \widetilde{x}} \bigg|_{\widetilde{x}=0} = 0, \quad \widetilde{c}(1) = \widetilde{c}_1,$$
(9)

$$\varepsilon_*^2 \widetilde{D}_N \frac{1}{\widetilde{r}} \frac{\partial}{\partial \widetilde{r}} \left(\widetilde{r} \frac{\partial \widetilde{c}_N}{\partial \widetilde{r}} \right) = 0, \quad \widetilde{c}_N(\widetilde{R}_p) = K_H \widetilde{c} \left(\widetilde{x} \right),$$

$$\varepsilon \varepsilon_*^2 \tilde{D}_N \frac{\partial \tilde{c}_N}{\partial \tilde{r}} \bigg|_{\tilde{r} = \tilde{R}_m} = -\tilde{c}_{N,m} \exp \tilde{\eta}$$
(10)

$$\varepsilon_*^2 \frac{\partial \tilde{j}}{\partial \tilde{x}} = -\tilde{c}_{N,m} \exp \tilde{\eta} \tag{11}$$

Here, $\tilde{c}_{N,m}$ and $\tilde{\eta}$ depend parametrically on \tilde{x} (see below). In Eq. (9), the dimensionless flux $\tilde{N}_{N,m}$ is given by

$$\tilde{N}_{N,m} = \frac{4Fl_t N_{N,m}}{\sigma_p b} = \tilde{D}_N \frac{\partial \tilde{c}_N}{\partial \tilde{r}} \bigg|_{\tilde{r} = \tilde{R}_m}, \tag{12}$$

the oxygen diffusion coefficients are normalized according to

$$\widetilde{D} = \frac{4FDc_{ref}}{\sigma_p b} \tag{13}$$

and ϵ , ϵ_* are the dimensionless parameters

$$\varepsilon = \frac{2\tilde{R}_m}{\tilde{R}_p^2}, \quad \varepsilon_* = \sqrt{\frac{\sigma_p b}{i_* l_t^2}}.$$
(14)

To find $\tilde{c}_{N,m}$ in Eq. (11) we solve Eq. (10):

$$\widetilde{c}_{N} = \begin{pmatrix} \widetilde{R}_{m} \ln \left(\widetilde{R}_{m} / \widetilde{r} \right) \exp \widetilde{\eta} + \varepsilon \varepsilon_{*}^{2} \widetilde{D}_{N} \\ \widetilde{R}_{m} \ln \left(\widetilde{R}_{m} / \widetilde{R}_{p} \right) \exp \widetilde{\eta} + \varepsilon \varepsilon_{*}^{2} \widetilde{D}_{N} \end{pmatrix} K_{H} \widetilde{c}.$$
(15)

Setting $\tilde{r} = \tilde{R}_m$ in this solution, we obtain

$$\widetilde{c}_{N,m} = \frac{K_H \widetilde{c}}{1 + \alpha \exp \widetilde{\eta}},\tag{16}$$

where $\alpha > 0$ is a constant parameter:

$$\alpha = \frac{\widetilde{R}_m}{\varepsilon \varepsilon_*^2 \widetilde{D}_N} \ln \left(\frac{R_m}{R_p} \right). \tag{17}$$

With this, Eq. (11) takes the form

$$\varepsilon_*^2 \frac{\partial \tilde{j}}{\partial \tilde{x}} = -\frac{K_H \tilde{c} \exp \tilde{\eta}}{1 + \alpha \exp \tilde{\eta}}.$$
 (18)

For further references we solve Eq. (18) for $\exp \tilde{\eta}$:

$$\exp \tilde{\eta} = -\frac{\varepsilon_*^2 \partial \tilde{j} / \partial \tilde{x}}{K_H \tilde{c} + \alpha \varepsilon_*^2 \partial \tilde{j} / \partial \tilde{x}}.$$
(19)

To eliminate $\tilde{\eta}$ from Eq. (18) we differentiate Eq. (18) over $\tilde{\eta}$, substitute $\exp \tilde{\eta}$ from Eq. (11) and use the Ohm's law $\tilde{j} = -\partial \tilde{\eta}/\partial \tilde{x}$. After simple algebra we come to

$$\frac{\partial^{2}\widetilde{j}}{\partial\widetilde{x}^{2}} - \left(\frac{\partial(\ln\widetilde{c})}{\partial\widetilde{x}} - \left(1 + \frac{\alpha\varepsilon_{*}^{2}}{K_{H}\widetilde{c}}\frac{\partial\widetilde{j}}{\partial\widetilde{x}}\right)\widetilde{j}\right)\frac{\partial\widetilde{j}}{\partial\widetilde{x}} = 0, \ \widetilde{j}\ (0) = \widetilde{j}_{0}, \widetilde{j}\ (1) = 0$$
(20)

Eq. (15) allows us to calculate the flux $\tilde{N}_{N,m}$, which appears in Eq. (9). Calculating derivative $\partial \tilde{c}_N/\partial \tilde{r}$, multiplying the result by \tilde{D}_N and setting $\tilde{r}=\tilde{R}_m$, we get

$$\tilde{N}_{N,m} = -\frac{K_H \tilde{c} \exp \tilde{\eta}}{\varepsilon \varepsilon_*^2 (1 + \alpha \exp \tilde{\eta})}$$

Using here Eq. (19), we come to

$$\tilde{N}_{N,m} = \frac{1}{\varepsilon} \frac{\partial \tilde{j}}{\partial \tilde{x}} \tag{21}$$

With this, Eq. (9) transforms to

$$\widetilde{D}_{ox} \frac{\partial^2 \widetilde{c}}{\partial \widetilde{x}^2} = -\frac{\partial \widetilde{j}}{\partial \widetilde{x}}, \quad \frac{\partial \widetilde{c}}{\partial \widetilde{x}} \bigg|_{\widetilde{x}=0} = 0, \quad \widetilde{c}(1) = \widetilde{c}_1,$$
(22)

Integrating this equation once, we find

$$\widetilde{D}_{\alpha x} \frac{\partial \widetilde{c}}{\partial \widetilde{x}} = \widetilde{j}_0 - \widetilde{j} , \quad \widetilde{c}(1) = \widetilde{c}_1, \tag{23}$$

which is a standard MHM equation for oxygen transport through the CCL depth.

Thus, the problem is reduced to the system of Eqs. (20), (23). With $\widetilde{f}(\widetilde{x})$ and $\widetilde{c}(\widetilde{x})$ at hand, the overpotential $\widetilde{\eta}$ is obtained from Eq. (19):

$$\tilde{\eta} = \ln \left(-\frac{\varepsilon_*^2 \, \delta \tilde{j} \, / \delta \tilde{x}}{K_H \, \tilde{c} \, + \, \alpha \varepsilon_*^2 \, \delta \tilde{j} \, / \delta \tilde{x}} \right) \tag{24}$$

and, if necessary, the radial shape of dissolved oxygen concentration \tilde{c}_N can be calculated from Eq. (15).

3. Results and discussion

Consider first the case of fast proton and oxygen transport along the

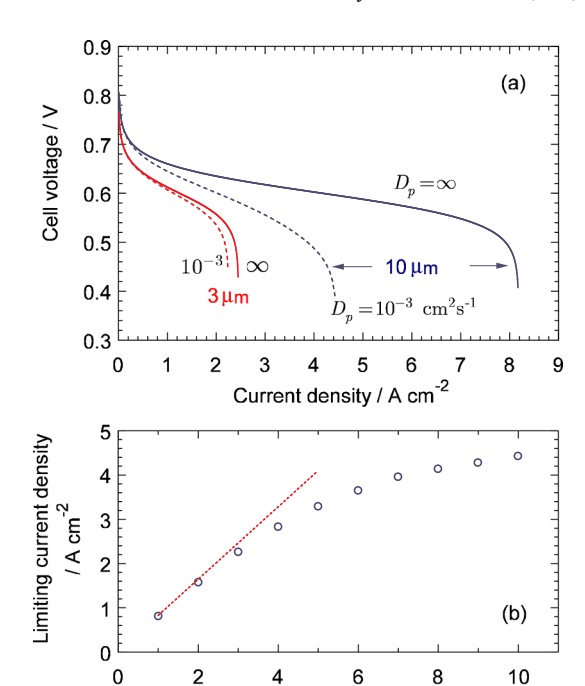


Fig. 2. (a) Polarization curves of the catalyst layer of the thickness $10\,\mu\mathrm{m}$ and $3\,\mu\mathrm{m}$. Solid lines, Eq. (26) (fast oxygen and proton transport), dashed lines, numerical solution to Eqs. (20), (23) (finite rates of proton and oxygen transport). All the curves are calculated as $V_{oc} - b\tilde{\eta}$, parameters for the calculation are given in Table 1. (b) Points: dependence of the limiting current density j_N^{lim} on the CCL thickness l_t calculated from the system of Eqs. (20), (23), dotted line: analytical solution, Eq. (28).

Catalyst layer thickness, µm

pore. In that case, the static oxygen concentration \tilde{c} and overpotential $\tilde{\eta}$ are nearly constant through the CCL depth. Integrating Eq. (18) over \tilde{x} from 0 to 1, we get

$$\varepsilon_*^2 \tilde{j}_0 = \frac{K_H \tilde{c} \exp \tilde{\eta}_0}{1 + \alpha \exp \tilde{\eta}_0},\tag{25}$$

where the subscript 0 marks the values at the membrane/CCL interface. Solving Eq. (25) for $\tilde{\eta}_0$ we get polarization curve of the CCL:

$$\widetilde{\eta}_0 = \ln \left(\frac{\varepsilon_*^2 \widetilde{j}_0}{K_H \widetilde{c} - \alpha \varepsilon_*^2 \widetilde{j}_0} \right) \tag{26}$$

Fig. 2a shows the polarization curves of the CCL of the thickness $10\,\mu\mathrm{m}$ and $3\,\mu\mathrm{m}$. Solid lines are calculated using Eq. (26), while the dashed lines result from numerical solution of the system of Eqs. (20), (23). The solid lines thus correspond to the fast rate of proton and oxygen transport in the CCL, while the dashed lines take into account finite rate of these processes.

As can be seen, all the curves demonstrate limiting current density. Eq. (26) helps to understand the effect: it exhibits the limiting current density \tilde{j}_N^{\lim} due to oxygen transport through the Nafion film. This current density makes the denominator in Eq. (26) equal to zero. With α from Eq. (17) and ϵ from Eq. (14), we find

$$\tilde{J}_{N}^{\text{lim}} = \frac{2\tilde{D}_{N}K_{H}\tilde{c}}{\tilde{R}_{p}^{2}\ln{(\tilde{R}_{m}/\tilde{R}_{p})}}.$$
(27)

In the dimension form this equation reads

$$j_N^{\text{lim}} = \frac{8FD_N l_t K_H c}{R_p^2 \ln(R_m/R_p)}.$$
 (28)

In the context of this work, most important is that j_N^{lim} is proportional to l_v i.e., the limiting current density due to oxygen transport through the Nafion film linearly decreases with the decrease in the CCL thickness.

Table 1Parameters used for calculation of the curves in Fig. 2. The ORR Tafel slope and the CCL proton conductivity are taken from impedance measurements [15].

Pore radius R_p , cm, Ref.[12]	$5 \cdot 10^{-6} (50 \text{nm})$
Nafion film thickness l_N , cm	$10^{-6} (10 \text{nm})$
Oxygen diffusion coefficient in	
the Nafion film, D_N , cm ² s ⁻¹ , Ref. [13]	10-6
Oxygen diffusion coefficient through	
the CCL depth, D_p , cm ² s ⁻¹ , Ref. [14]	10^{-3}
* · · · ·	
Exchange current density i*, A cm ⁻³ (assumed)	10 ⁻³
ORR Tafel slope b, V	0.03
CCL proton conductivity σ_p , Ω^{-1} cm ⁻¹	0.03
Henry constant (mol/mol)	$6.76 \cdot 10^{-3}$
Cell temperature T, K	273 + 80
•	

This may explain unexpected poor performance of the low–Pt catalyst layers. Indeed, lower Pt loading means proportional decrease in the CCL thickness. For example, the standard CCL with the Pt loading of 0.4 mg cm $^{-2}$ is four times thicker, than the CCL with the Pt loading of 0.1 mg cm $^{-2}$. Note that all the other parameters appearing in Eq. (28) are the same for the thick and thin CCLs.

Formally, the polarization curve of the CCL with negligible voltage loss in the Nafion film can be obtained from Eq. (26) by setting $\alpha=0$, which leads to the Tafel law. As can be seen, oxygen transport in the Nafion film leads to much faster decay of $\tilde{\eta}_0$ with \tilde{j}_0 , as compared to the Tafel equation.

The fact that $j_N^{\rm lim}$ decreases with the CCL thickness l_t (with Pt loading) explains the over–linear dependence discussed above. Fig. 2b compares the dependence of $j_N^{\rm lim}$ on the CCL thickness l_t calculated numerically from Eqs. (20), (23) with the analytical result Eq. (28). Note that Eq. (28) well describes the numerical result for the CCL thickness below $3 \, \mu \rm m$.

The model above could be completed with the oxygen transport in the GDL. This would lead to another limiting current density j_{GDL}^{lim} due to finite oxygen diffusivity of the GDL. Thus, we may face the situation when in the standard CCL, j_N^{lim} exceeds j_{GDL}^{lim} and the effect of oxygen transport through the Nafion film is not seen, while in the low–Pt CCL, several times lower j_N^{lim} may limit the cell polarization curve.

Qualitatively, the oxygen transport path from the CCL/GDL interface to the Pt surface consists of two consecutive steps: the transport in the void pore followed by the transport through the Nafion film. The shorter the pore, the larger the weight of the transport in Nafion in the overall balance of oxygen fluxes. This explains proportionality $j_N^{\rm lim} \sim l_t$ in Eq. (28).

Finite through–plane oxygen diffusion coefficient D_p strongly affects the shape of the curve in the thick 10– μ m CCL, while in the thin 3– μ m CCL, the effect of D_p on the limiting current density is marginal (Fig. 2).

To rationalize the dependence of $j_N^{\rm lim}$ on the pore radius R_p we will assume that R_p is much larger than the Nafion film thickness l_N . Thus, $\ln{(R_m/R_p)} = \ln{(1+l_N/R_p)} \simeq l_N/R_p$. Substituting this relation into Eq. (28) we get

$$j_N^{\text{lim}} = \frac{8FD_N l_t K_H c}{R_p l_N} \tag{29}$$

Thus, another useful hint from Eq. (29) is that $j_N^{\rm lim} \sim R_p^{-1}$, i.e., lowering of the mean pore radius in the CCL increases $j_N^{\rm lim}$, making the cell polarization curve less sensitive to oxygen transport in the Nafion film. Physically, lowering of R_p means reduction of the total proton current entering the pore, as another pore takes over part of the current for the conversion.

No attempts to fit the numerical polarization curve following from Eqs. (20), (23) to the experimental curves available in literature have been done. The problem is that the effective oxygen diffusion

coefficient in the CCL D_{ox} , which is a composite containing D_p and D_N strongly depends on the cell current density [15]. A much better alternative to validate the model above is impedance spectroscopy. This, however, requires development of a transient analog of the model, which will be reported in a full-length paper.

4. Conclusions

A single–pore model for the cathode catalyst layer performance in a PEM fuel cell is developed. The model takes into account oxygen transport through the CCL depth and through the Nafion film covering Pt/C agglomerates. In the limit of fast proton and through–plane oxygen transport in the CCL analytical solution for the CCL polarization curve is derived. This solution reveals a limiting current density due to proton transport through the Nafion film j_N^{lim} . Moreover, j_N^{lim} is proportional to the CCL thickness l_i ; thus, in the low–Pt CCL, due to its much lower thickness, the effect of oxygen transport through the Nafion film may limit the cell current density. Another useful hint from the analytical result is inverse proportionality of j_N^{lim} to the mean mesopore radius R_p , meaning that the CCL with lower R_p is less sensitive to oxygen transport through the Nafion.

Nomenclature

~	Marks dimensionless variables
b	
υ	ORR Tafel slope, V
c	Oxygen molar concentration in the pore, mol cm^{-3}
c_{ref}	Reference oxygen concentration, mol cm ⁻³
D_p	Oxygen diffusion coefficient in the pore, $cm^2 s^{-1}$
D_N	Oxygen diffusion coefficient in the Nafion film, cm ² s ⁻¹
F	Faraday constant, C mol ⁻¹
j	Local proton current density along the pore, A cm ⁻²
$j_N^{ m lim}$	Limiting current density due to oxygen transport in Nafion
	film, A cm ⁻²
j_0	Cell current density, A cm ⁻²
i*	Volumetric exchange current density, A cm ⁻³
l_t	Catalyst layer thickness, cm
l_N	Nafion film thickness, cm
R_m	Radius of a Pt/C tube, cm
R_p	Pore radius, cm
r	Radial coordinate, cm
x	Coordinate through the CCL, cm

Subscripts

0	Membrane/CCL interface
1	CCL/GDL interface
t	Catalyst layer

Greek

α	Dimensionless parameter, Eq. (17)					
ϵ	Dimensionless 1	Newman's	reaction	penetration	depth,	Eq.
	(14)					
ϵ	$2\tilde{R}_m/\tilde{R}_p^2$					

References

- [1] T. Grezler, D. Gaulk, P. Sinha, J. Electrochem. Soc. 159 (2012) F831-F840.
- [2] A. Kongkanand, M.F. Mathias, Phys. Chem. Lett. 7 (2016) 1127-1137.
- [3] J.P. Owejan, J.E. Owejan, W. Gu, J. Electrochem. Soc. 160 (2013) F824-F833.
- [4] A.Z. Weber, A. Kusoglu, J. Mater. Chem. A 2 (2014) 17207-17211.
- [5] M.-J. Choo, K.-H. Oh, J.-K. Park, H.-T. Kim, ChemElectroChem 2 (2015) 382–388.
- [6] K. Kudo, R. Jinnouchi, Y. Morimoto, Electrochim. Acta 209 (2016) 682–690.
- [7] M. Moore, P. Wardlaw, P. Dobson, J.J. Boisvert, A. Putz, R.J. Spiteri, M. Secanell, J. Electrochem. Soc. 161 (2014) E3125–E3137.

- [8] L. Hao, K. Moriyama, W. Gu, C.-Y. Wang, J. Electrochem. Soc. 162 (2015) F854-F867.
- [9] T. Mashio, H. Idena, A. Ohma, T. Tokumasu, J. Electroanal. Chem. 790 (2017) 27-39.
- [10] L. Chena, R. Zhang, P. He, Q. Kang, Y.-L. He, W.-Q. Tao, J. Power Sources 400 (2018) 114-125.
- [11] P. Dobson, C. Lei, T. Navessin, M. Secanell, J. Electrochem. Soc. 159 (2012)

B514-B523.

- [12] M. Eikerling, J. Electrochem. Soc. 153 (2006) E58-E70.
- [13] V.A. Sethuraman, S. Khan, J.S. Jur, A.T. Haug, J. Weidner, Electrochim. Acta 54 (2009) 6850–6860.
- [14] J. Shen, J. Zhou, N.G.C. Astrath, T. Navessin, Z.-S.S. Liu, C. Lei, J.H. Rohling, D. Bessarabov, S. Knights, S. Ye, J. Power Sources 96 (2011) 674–678.

 [15] T. Reshetenko, A. Kulikovsky, J. Electrochem. Soc. 163 (2016) F1100–F1106.